Automatic Stub Avoidance for a Powered Prosthetic Leg over Stairs and Obstacles

Shihao Cheng, Curt A. Laubscher, and Robert D. Gregg

Abstract—Passive prosthetic legs require undesirable compensations from amputee users to avoid stubbing obstacles and stairsteps. Powered prostheses can reduce those compensations by restoring normative joint biomechanics, but the absence of user proprioception and volitional control combined with the absence of environmental awareness by the prosthesis increases the risk of collisions. This paper presents a novel stub avoidance controller that automatically adjusts prosthetic knee/ankle kinematics based on suprasensory measurements of environmental distance from a small, lightweight, low-power, low-cost ultrasonic sensor mounted above the prosthetic ankle. In a case study with two transfemoral amputee participants, this control method reduced the stub rate during stair ascent by 89.95% and demonstrated an 87.5% avoidance rate for crossing different obstacles on level ground. No thigh kinematic compensation was required to achieve these results. These findings demonstrate a practical perception solution for powered prostheses to avoid collisions with stairs and obstacles while restoring normative biomechanics during daily activities.

Fig. 1. (A) Conceptual diagram of the stub avoidance controller based on the ultrasonic sensor distance measurement (d_{st}) during stance phase for both stair ascending and obstacle crossing. Extra knee ($\Delta\theta_{kne}$) and ankle ($\Delta\theta_{ank}$) flexions are applied based on an inverse relation of measured distance to prevent prosthetic foot stubbing. (B) Block diagram of the position controller with distance-based kinematics modification. In the baseline controller, gait phase (ϕ) is estimated in real-time with fixed task variables (χ) to generate reference angles for the knee and ankle joints using data-driven kinematics models [23]. The stub avoidance controller modifies the reference joint angles based on d_{st}. Joint torques are generated with a proportional–integral–derivative position controller based on the reference joint angles.

I. INTRODUCTION

Passive prosthetic legs enable individuals with lower-limb loss to perform daily activities such as level walking (LW). However, these devices require significant compensations (e.g., hip hiking, hip circumduction, and/or vaulting) from the user to achieve foot clearance [1]. The lack of precise control and proprioception contributes to a high rate of stumbles, trips, and falls for transfemoral prosthesis users [2]–[4]. Passive devices also cannot provide the positive mechanical work needed for activities such as ramp ascent and stair ascent (SA), which are only possible with additional compensations from intact joints [5], [6]. The associated overuse of intact joints increases the risk of secondary musculoskeletal injuries in the amputee population [7]. Emerging powered prostheses have demonstrated advantages over passive or quasi-passive devices by providing net-positive mechanical work and active control [8]–[12].

Powered prostheses typically replicate normative able-bodied (AB) joint kinematics and/or kinetics using sensor feedback analogous to biological proprioception (e.g., joint angles, limb angles, loads) [13]. While this control philosophy can improve prosthesis biomimicry and gait symmetry [14]–[16], these devices generally lack higher-level perception to adjust the joint trajectories to risky foot placements on stairs
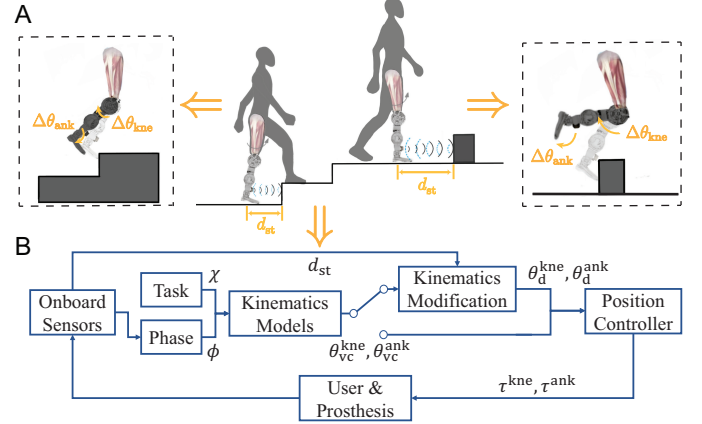
S. Cheng, C. Laubscher, and R. Gregg are with the Department of Robotics, University of Michigan, Ann Arbor, MI, 48109 USA. Contact: {chengsh, claub, rdgregg}@umich.edu

(e.g., too close to the next stairstep) or sudden changes in walking surface height (e.g., due to a curb or obstacle) [17]. In fact, one study reported a substantially higher rate of falls with the commercial Össur Power Knee II than a mechanical knee [18], despite participants having higher balance confidence with the powered device. One possible explanation is that normative joint kinematics, while more efficient, naturally provide less foot clearance than compensatory motions (e.g., mean of 15 mm [19] vs. 34.1 mm [20], respectively, during LW), thus increasing the risk of stubbing in uncertain environments. In contrast, the combination of proprioception and vision allows AB individuals to make subtle adjustments to swing knee kinematics and toe trajectories based on their foot position relative to stairsteps or obstacles. Proper foot placement can reduce the risk of stubs, trips, and falls on stairs [21], but this is especially hard for prosthesis users who lack proprioception and volitional control over the prosthesis [22].

Although many stumble recovery strategies have been proposed for powered prosthetic legs [4], [24]–[26], recent studies have focused on actively avoiding such events. Rezazadeh et al. [14] enabled obstacle crossing using a phase variable-based position controller, in which the user's residual thigh motion controls the prosthetic joint's progression through nominal AB walking kinematics. By holding their hips in an extended

position, the user was able to freeze the prosthetic knee in a flexed position and then circumduct the leg over the obstacle. However, this method requires an unnatural compensation to cross an obstacle, and the maximum obstacle height is limited by the maximum knee flexion during LW. Gordon et al. [27] also utilized thigh kinematics as features for machine learning to predict obstacle crossing intent after toe-off (TO) and subsequently adjust the knee and ankle flexion, but the method could only detect obstacles with 83% sensitivity. Mendez et al. [17] enabled crossing obstacles of variable heights by adjusting maximum knee flexion based on the time-integral of the user's residual thigh motion. However, this approach requires the user's hip to unnaturally hold the weight of the prosthesis in an extended position over time to get extra knee flexion, requiring a longer swing period for taller obstacles. The same group enabled SA over different stairstep heights by adjusting the prosthesis swing kinematics based on the user's residual thigh motion [28]. However, this method also requires specific hip motions to provide adequate toe clearance, and the controller's dependence on thigh velocity and acceleration makes it susceptible to inertial sensor noise.

While the above methods use common inertial sensors on powered prostheses, suprasensory environmental perception could potentially detect obstacles to avoid collisions without intact joint compensations. For example, environmental features collected by a laser distance meter [29], RGB camera [30]–[32], depth camera such as LiDAR [33], or the fusion of camera and inertial sensors [34], [35] have been utilized to recognize the approaching terrain with high accuracy for prosthesis control. The depth camera in [34] calculated the vertical distance between the prosthetic foot and the top of the obstacle so that extra knee flexion can be applied to provide enough clearance to cross over obstacles up to 0.3 m in height. However, the method required the user to significantly slow down the walking speed to accommodate the computational latency of processing the point cloud data. Thatte et al. [36] used LiDAR mounted above the knee to measure ground distance, allowing real-time optimization of swing kinematics to avoid early foot contact (FC) during LW. However, this method was not tested for crossing obstacles or stairs. None of these methods account for varying foot placements during SA to actively avoid stubbing the stairs.

Fortunately, there is an emerging opportunity to implement real-time stub avoidance on powered prostheses as the size, weight, power consumption, computational load, and cost of environmental perception modalities continue to improve. For example, RGB and LiDAR cameras have become more affordable and lighter (e.g., LiDAR introduced to the Apple iPhone 13 Pro), but they still face limitations for the prosthetic use case such as high computational time [37], sensitivity to motion [38] and environmental conditions (e.g., rain or fog) [39], and Lambertian assumptions making them less effective with transparent or light-reflective objects [40]. Alternatively, ultrasonic sensors are even cheaper, lower power, and more computationally efficient, and a wide range of outdoor applications [41] from automotive [42] to smart wheelchairs [43] have demonstrated their ability to quickly and accurately measure distances to close objects.

This paper presents an ultrasonic sensor-based method to automatically modify the nominal kinematic trajectories of a powered knee-ankle prosthesis for stub avoidance, without requiring residual limb compensations. We mounted a single ultrasonic sensor above the prosthetic ankle joint to detect the distance to the upfront terrain. Based on these measurements, our stub avoidance scheme (Fig. 1(A)) introduces extra knee and ankle flexion to a baseline, phase-based controller (Fig. 1(B)) that restores normative joint kinematics according to a continuous data-driven model of LW and SA [23]. To determine risky stepping conditions that require active stub avoidance, we simulated nominal AB kinematics during SA with different foot placements relative to the next stairstep. We evaluated the efficacy of the stub avoidance controller by conducting a case study with two transfemoral amputee (TF) participants using a powered knee-ankle prosthesis during 1) SA with risky foot placement and 2) LW obstacle crossing. The stub avoidance controller reduced the stair stub rate by 89.95% compared to the baseline controller, without requiring excessive hip flexion seen with passive prosthetic devices. These participants also demonstrated an 87.5% stub avoidance rate during LW obstacle crossing, without requiring excessive hip motions. Finally, we performed an offline simulation using pre-recorded ultrasonic data over a multi-activity circuit to show a false positive (FP) activation rate of 1.23%, demonstrating the robustness of the stub avoidance controller in real-world scenarios.

The rest of this paper is organized as follows. Section II introduces the risky foot placement analysis for SA, the baseline controller for SA and LW, the stub avoidance controller, and the experimental and simulation methods to validate controller performance. Section III summarizes the results of the experiments in terms of the baseline controller's ability to restore normative joint biomechanics and the reduced stub rate with the avoidance controller compared to the baseline. Section IV discusses these results and explores possible future studies. Finally, we conclude in Section V.

II. METHODS

This section summarizes how we designed and validated the stub avoidance controller during LW and SA. To first determine when automatic stub avoidance is needed, we start with an offline simulation using motion capture data to determine when the foot is placed close enough to the next stairstep to cause a stub event using nominal AB joint kinematics. Next, we introduce the powered prosthetic leg used for this study, followed by the description of the control framework for both baseline and stub avoidance controllers. We then describe the experiment procedure to validate the performance of both controllers during LW and SA and assess the robustness with a multi-activity simulation. Finally, we introduce the method for analyzing the experimental data.

A. Stub Risk Stepping Condition in Stair Ascent

We define a clear step during SA as a step where the toe trajectory never intersects with the stairs (either the first or second stair step for step-over-step gait) during the swing
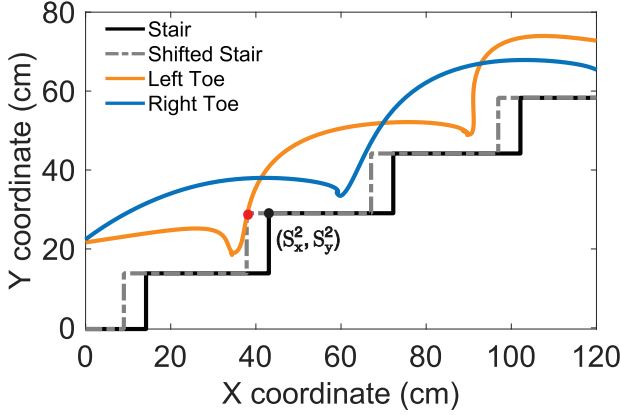
Fig. 2. Toe trajectories for stair ascending. Example toe trajectories for a single subject for both left (solid red) and right (solid blue) legs and the staircase (solid black) at 30° incline are shown in the figure. The grey dashed line represents the shifted staircase based on the minimum horizontal distance between the trajectory and stairstep from the simulation result. The red dot indicates the left toe trajectory intersects with the shifted staircase to simulate the situation when the foot is placed very close to the next stairstep.

phase, whereas a stub step does. An intersection can occur in the early swing phase with the first stairstep or the late swing phase with the second stairstep during step-over-step SA. The knee and ankle joints of powered prostheses often follow predefined kinematic patterns (time-invariant AB trajectories in our case), so the resulting toe trajectories do not change based on the foot placement on the stair tread. To determine the reference safe distance between the prosthetic foot and the next stairstep to avoid stubbing, pre-recorded motion capture data [44] was simulated by plotting the static stair markers with horizontal shifts towards the toe trajectories. For example, Fig. 2 plots the left and right toe trajectories against the stair markers at 30° incline (14.6 cm riser height, 29.5 cm tread depth). To determine when the toe trajectory would intersect/stub with the stairstep, we calculated the minimum horizontal (x-axis) distance between the toe trajectory and the stairstep edge when the trajectory is below the stairstep height using

$$d_{\min} = \min\{S_x^c - T_x(t) \mid \forall t, S_y^c > T_y(t)\}, \qquad (1)$$

where $T_x(t)$ and $T_y(t)$ are time-dependant x- and y-coordinates of the toe trajectory, respectively, throughout the swing phase. For the cth stairstep edge for $c \in \{1, 2, 3, 4\}$, S_x^c and S_y^c represent the x- and y-coordinate, respectively.

Once we found the minimum distance, we shifted the x-coordinate towards the toe trajectory by the same amount, which is shown as the grey dashed line in Fig. 2 to mimic the situation when the toe stubs the stair if the foot is placed $d_{\min}$ amount of distance closer to the stair. By simulating across multiple trials of experiment data at the same incline over different subjects, we found the mean safe distance to SA without stubs is 9.6 cm (3.8 inches).

B. Powered Knee-Ankle Prosthesis

This study used the powered knee-ankle prosthesis designed in [11] as shown in Fig. 4. The prosthesis is equipped

with low-impedance actuators capable of producing high torque through a custom 22:1 single-stage stepped-planet compound planetary gear transmission. It uses G-SOLO Twitter R80A/80VDC drivers (Elmo Motion Control, Petah Tikva, Israel) to power the motors. The actuators are capable of precise position control [11] with enough torque/power to perform demanding activities such as SA [45]. The control and signal processing code runs on a myRIO 1900 (National Instruments, Austin, TX) at 500 Hz, and the prosthesis is powered by four lithium-polymer batteries connected in series. The residual thigh's global orientation is measured using a 3DM-CX5-25 (LORD Microstrain, Williston, VT) inertial measurement unit (IMU), and motor positions are measured using E5 optical quadrature encoders (US Digital, Vancouver, WA) with velocities estimated using Savitzky-Golay differentiation. The prosthetic foot is mounted under a 6-axis load cell (M3564F, Sunrise Instruments, Nanning, China) at the distal end of the ankle joint.

Unique to this study, an ultrasonic distance sensor (LV-MaxSonar-EZTM, MaxBotix, Brainerd, MN) is attached above the ankle on the shank. This ultrasonic sensor costs $34 (US dollars), sizes 19.9×22.1×15.5 mm, weighs 4.3 g, consumes 11 mW, and samples at a maximum frequency of 40 Hz. Although cutting-edge LiDARs may provide more information to sense objects in front of the device by constructing point clouds (e.g., CamBoard pico flexx, PMD Technologies [34]), it is more expensive ($399), larger in size (68×17×7.35 mm), weight (8 g), and power consumption (540-680 mW), while having comparable sampling time (> 30 ms). As another example, the LiDAR in the iPhone 13 Pro (Apple Inc., Cupertino, CA) depends on the light and environment conditions (e.g., weak in sensing transparent objects) and is sensitive to motion [38]. Alternatively, computer vision with an RGB camera can also collect more information from the environment but is subject to similar disadvantages to LiDAR with even higher computational time [37]. Thus, we believe an ultrasonic sensor, which can timely and accurately measure the distance to the upfront terrain, is sufficient for our application considering the known limitations of the alternative options.

C. Control Framework

The proposed controller is summarized in the block diagram shown in Fig. 1(B). The stub avoidance controller, which applies kinematics modification when on, adjusts the desired kinematics enforced by the baseline controller. We first describe this baseline controller and then discuss the kinematics modification in the stub avoidance controller.

1) Baseline Controller: The baseline controller enforces virtual kinematic constraints [46] at the knee and ankle joints determined by the kinematics models in our previous work [23]. These models were derived from averaged joint kinematics from an AB dataset for walking and stair climbing. The models return the desired joint angle θ_d^j and velocity $\dot{\theta}_d^j$ for joint $j \in \{\text{kne}, \text{ank}\}$, which are continuous functions of task and phase variables. Task contains the inclination and forward speed on ground or stairs, which can be determined in real-time [16] but were fixed in this study for simplicity (1 m s^{-1} for both SA and LW, and 26.5° for SA and 0° for LW).

The phase variable is estimated from the global thigh orientation (measured by an onboard thigh IMU) as originally proposed in [47]. Phase variable definitions have been extended from LW [46] to ramp walking [16] and stair climbing [45], but these recent definitions only considered two monotonic sections of the thigh trajectory (descending and ascending corresponding to S1 and S2 in Fig. 3(A)). These definitions typically ignore or feedforward the second descending portion of the thigh trajectory (S3 in Fig. 3(A)), thus diminishing the user's volition over gait progression. Cortino et al. [45] and Hong et al. [48] solved this problem by redefining the gait cycle to start and end at maximum hip flexion (MHF) rather than heel strike (HS), but this approach is sensitive to accurate and timely MHF detection in real-time.

Therefore, we propose a different definition by defining an extra descending state (S3) between MHF and HS, based on an estimate of the thigh angle at HS, see Fig. 3(A). The phase variable (ϕ) can then be calculated as follows based on the state of the thigh trajectory:

$$\phi = \begin{cases} \frac{\theta_{th}^{HS} - \theta_{th}}{\theta_{th}^{HS} - \theta_{th}^{MHE}} \phi^{MHE} & \text{if } S1, \\ \phi^{MHE} + \frac{\theta_{th} - \theta_{th}^{MHE}}{\theta_{th}^{MHF} - \theta_{th}^{MHE}} \left(\phi^{MHF} - \phi^{MHE} \right) & \text{if } S2, \\ \phi^{MHF} + \frac{\theta_{th}^{MHF} - \theta_{th}}{\theta_{th}^{MHF} - \theta_{th}^{HS}} \left(1 - \phi^{MHF} \right) & \text{if } S3, \end{cases} \quad (2)$$

where θ_{th}^{HS} and θ_{th}^{TO} are the thigh angle at HS and TO, respectively. The coordinates $(\theta_{th}^{MHE}, \phi^{MHE})$ and $(\theta_{th}^{MHF}, \phi^{MHF})$ represent the (thigh angle, phase) pair at the maximum hip extension (MHE) and MHF, respectively. In pilot experiments, some participants tended to swing the prosthetic legs backward after TO, causing the MHE to occur later than TO. To avoid the associated phase lag, we allow the phase to jump from the current value to the expected TO phase ϕ^{TO} using the mean value from the AB dataset [44]. To ensure the phase is continuous, we use a second-order Butterworth low-pass filter (200 rad/s natural frequency, 0.9 damping ratio) to smooth the jump if MHE occurs later than TO and replace the governing equation in $S2$ with

$$\phi = \phi^{TO} + \frac{\theta_{th} - \theta_{th}^{TO}}{\theta_{th}^{MHF} - \theta_{th}^{TO}} (\phi^{MHF} - \phi^{TO}). \quad (3)$$

A finite-state machine (FSM) is used to select and transition from the three segments S1, S2, and S3, depending on measurements and detection of the critical gait events. Because the thigh angle is not always as clean as depicted in Fig. 3(A) (e.g., could have additional local extrema resulting in extra monotonic sections), the FSM is implemented to transition not only sequentially between the three segments but also to permit backtracking of the state when false detections occur. The logic for this FSM is summarized in Fig. 3(B), where the real-time method for detecting MHF and MHE is described in our prior work [49]. The S1 to S2 transition can happen if either MHE or early TO is detected. In S2, we allow the transition back to S1 if the thigh angle is found to decrease while there is FC. If MHF is detected, the FSM transitions to S3. In S3, the FSM can transition back to S2 if the thigh angle exceeds MHF. Finally, the FSM can transition into S1 from S3 once HS is detected.
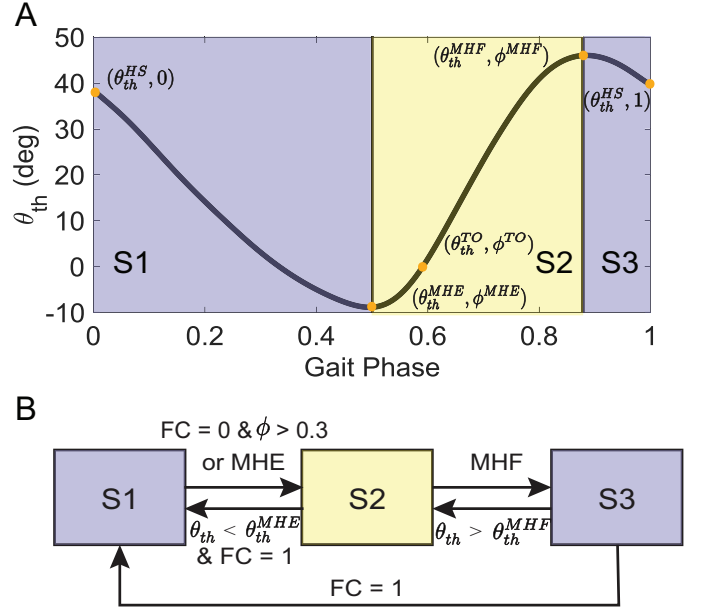

Fig. 3. Phase definition and state-machine-based transition logic. (A) The phase variable (ϕ) during level walking and stair ascending is based on the thigh orientation angles in the sagittal plane (θ_{th}). The gait cycle contains three sections: first descending S1, ascending S2, and second descending S3. The yellow dots represent critical gait events of heel strike (HS), maximum hip extension (MHE), toe-off (TO), and maximum hip flexion (MHF). Each bracket contains the corresponding thigh angle and phase at those gait events. (B) Flow chart depicting the gait segments and transition logic for the finite-state machine. Forward transitions (S1 → S2 → S3 → S1) are determined from gait features and foot contact (FC), and reverse transitions (S3 → S2 → S1) occur after false detections are determined.

The baseline controller tracks the reference joint angles provided by the virtual constraints using a proportional–integral–derivative (PID) position controller. The PID controller commands motor torque by

$$\tau^j = k_p^j \left(\theta_d^j - \theta^j \right) + k_i^j \int \left(\theta_d^j - \theta^j \right) dt + k_d^j \left(\dot{\theta}_d^j - \dot{\theta}^j \right) \quad (4)$$

where θ^j and $\dot{\theta}^j$ are the measured joint angle and velocity, respectively, and k_p^j, k_i^j, and k_d^j are the (constant) proportional, integral, and derivative gains (see Table S2). These gains were determined iteratively during pilot trials to maximize the tracking performance of each joint without providing excessive torques. Note larger proportional and integral gains are needed to support and push up the user's weight during the stance phase compared to swing. The same set of gains was used for both LW and SA and for both participants.

2) Stub Avoidance Controller: A conceptual diagram of the stub avoidance controller is shown in Fig. 1(A). The controller modifies the desired joint angles from the kinematic models in Fig. 1(B), where the switch enables the kinematics modification. This adjustment is based on the ultrasonic sensor's distance measurements to determine how much extra knee flexion and ankle plantarflexion are needed to clear a stairstep or obstacle. The modified knee and ankle reference angles, θ_d^{kne} and θ_d^{ank}, are calculated based on the real-time measurement distance during each stance phase:

$$\theta_d^{kne} = \theta_{vc}^{kne} + \Gamma \left[k_{kne} \cdot \langle d_{safe} - d_{st} \rangle \right] \quad (5)$$

$$\theta_{\mathrm{d}}^{\mathrm{ank}} = \theta_{\mathrm{vc}}^{\mathrm{ank}} + \Gamma\left[k_{\mathrm{ank}} \cdot \langle d_{\mathrm{safe}} - d_{\mathrm{st}}\rangle\right] \qquad (6)$$

where $\theta_{\mathrm{vc}}^{\mathrm{kne}}$ and $\theta_{\mathrm{vc}}^{\mathrm{ank}}$ are the desired knee and ankle angles from the kinematics models described previously [23]. d_{st} is the minimum distance measured from the ultrasonic sensor during the most recent stance phase, and d_{safe} is a safe distance chosen later. $\langle \cdot \rangle$ denotes a rectifier, returning its value only when the value is positive and zero otherwise. The proportional gains, k_{kne} and k_{ank}, were tuned during pilot sessions to achieve the prosthetic knee joint's maximum flexion angle after measuring zero distance between the prosthetic toe and an obstacle, allowing clearance of the highest obstacle in our laboratory. These gains were also proven effective in navigating the steepest stair inclination without stubs. During these pilot trials, we found that ankle plantarflexion creates more ground clearance than dorsiflexion for both stair ascending and obstacle crossing, which matches with the changes in ankle flexion reported in [17] during obstacle crossing. Therefore, k_{ank} is chosen to be negative to generate ankle plantarflexion. $\Gamma[\cdot]$ is a second-order Butterworth low-pass filter that is only applied to the extra flexion term. This filter is necessary to reduce the instability potentially caused by the step response of flexion, especially when the flexion amount is large (i.e., foot placed very close to the obstacle/stairs $d_{\mathrm{safe}} \gg d_{\mathrm{st}}$). The Butterworth filter (20 rad/s natural frequency, critically damped) was chosen to keep the original slope of joint angles before and after the flexion occurs. The kinematics modification applies immediately after the TO and disengages when the phase is greater than 0.8, giving the leg enough time to extend to the desired position to prepare for the HS.

For SA, the safe distance $d_{\mathrm{safe}} = 26$ cm was determined by adding 1) $d_{\mathrm{min}} = 9.6$ cm from Section II-A, 2) the fixed distance between the sensor and the toe (15.24 cm), and 3) about 1 cm margin of safety to avoid stubs when the foot is placed near but behind the line. For obstacle crossing in LW, d_{st} is the minimum distance measured during stance when the global shank orientation is greater than $-5°$ from vertical, and $d_{\mathrm{safe}} = 55$ cm was chosen during pilot sessions based on the comfortable step length to step over the obstacle. All gains and parameters are summarized in Table S2.

D. Experimental Protocol

The study involved two TF participants using the powered knee-ankle prosthesis designed in [11]. Table S3 summarizes participant anthropometrics and other general information. The University of Michigan Institutional Review Board granted approval for the research protocol on August 28, 2020, with protocol number HUM00166976. Each subject provided written informed consent before the experiment. At the beginning of each experiment, the powered prosthetic leg was fit by a licensed prosthetist with proper alignment. Both participants had more than 5 hours of experience using the powered prosthesis prior to the experimental study conducted in this paper. The participants were trained with the new controller for at least 2 hours prior to data collection. During this time, the stair inclination was set to $26.5°$ for both participants based on their comfort.
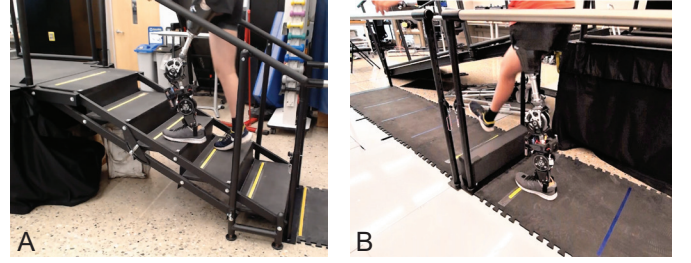

Fig. 4. Experiment Setup. Experimental setup for both (A) stair ascending, and (B) obstacle crossing to validate the baseline and stub avoidance controller. (A) Yellow tapes are placed on each stair to indicate the safe line without stubbing from the simulation results. The participants are asked to step in front of or behind the yellow line during stair ascending to induce or prevent stubs, respectively. (B) The black rectangular bar is used as the obstacle with yellow tapes in front of and behind to indicate the region for foot placement based on the comfortable step length to step over the obstacle from the acclimation trials.

The experimental setup for stair stub avoidance is shown in Fig. 4(A). The safe distance from the edge of each stairstep found in Section II-A was indicated using yellow strips of tape on the stairs. A step in front of the line (close to the next stairstep) means the participant has a high stub risk, while a step behind the line (far from the next stairstep) means low risk. We turned the stub avoidance controller (kinematics modification) on or off for different trials to compare the kinematics and stub rate of the prosthetic leg with and without the extra joint flexion. To minimize bias from the participants, they were not informed whether the stub avoidance controller was turned on or off. Four conditions in total were considered for this experiment: 1) step close with the controller, 2) step far with the controller, 3) step close without the controller, and 4) step far without the controller. At the beginning of each trial, we instructed the participant to step either close or far on the stairs, and actual step placement relative to the line was recorded by the side camera and manually marked during post-processing. We performed 48 trials in total with those four conditions assigned randomly with an equal number for each. A mandatory 2–5 minute break was given every 8 trials. To minimize transients and obtain stair kinematics more representative of a steady-state activity, the participants started each trial with at least one LW stride before transitioning to SA. Similarly, to avoid a sudden stop on the last stair step, they were instructed to transition and continue after the SA for some LW strides. The stub avoidance controller was only used during SA, and the participant walked at their own self-selected pace. The stair steps were video recorded for later processing to determine stub events.

The obstacle crossing setup is shown in Fig. 4(B). A box with dimensions $60.3 \times 12.1 \times 17.1$ cm was placed in the middle of the parallel bars walkway. Yellow strips of tape were placed an average step length away from the obstacle on both sides to improve foot placement consistency when crossing the obstacle. For each trial, the participant walked at least one stride with the prosthetic leg before and after crossing the obstacle, leading with the healthy leg during the crossing. Participants performed 8 trials with each obstacle height (12.1 cm and 17.1 cm), taking a 2–5 minute break between different obstacle heights.

E. Multi-Activity Simulation

To evaluate the robustness of the proposed method (i.e., FP rate for triggering extra flexion) during daily activities, we simulated the stub avoidance controller using ultrasonic measurements from a pre-recorded multi-activity dataset from our prior work [50], which includes sit-stand, level/ramp walking, turning, stair ascent/descent, and continuous transitions between those activities. The data comes from an experiment conducted with TF01 using the same hardware setup, including the ultrasonic sensor. The participant was instructed to perform the above activities continuously in a relatively narrow laboratory full of chairs, desks, and parallel bars, which introduced challenges for triggering unnecessary extra flexions. In this simulation, we assume perfect activity classifications and ground slope estimation. We classified false events by extra flexion greater than $3.56°$ for the knee and $2.33°$ for the ankle, which correspond to the minimal perceptible changes in those joint angles by AB [51], [52].

We made several changes to the distance-measuring method to accommodate the additional complexity of this environment without affecting the performance of the stub avoidance controller in the previously described SA and LW scenarios. Instead of taking the minimum distance d_{st} when the global shank orientation is greater than $-5°$ from vertical during stance, we used a moving average filter with a 10-sample window to calculate the mean distance when the shank is within a small angle threshold of being perpendicular to the ground during each stance. In addition, we used the distance history to check whether the participant is approaching the obstacle by comparing the distance from the last stride d_{st}^{t-1} with the current stride d_{st}^t. The extra flexion is only triggered if 1) $d_{st}^{t-1} > d_{st}^t + d_{safe}$, and 2) $d_{st}^t < d_{safe}$. Finally, we classify turning based on the roll, pitch, and yaw measurement from the thigh IMU within one stride and void the distance measurement if the heading direction is changed by more than $30°$ within a stride. To ensure these controller adjustments would not invalidate this paper's real-time results, we also ran a simulation with the obstacle-crossing experiment data and confirmed the extra flexion before and after the changes are comparable for each trial.

F. Data Analysis

To assess the biomimicry of the baseline controller for both LW and SA, we compared the logged prosthetic-side kinematics during steady-state gait (without extra flexion) to mean AB kinematic data [44], which we quantified using the mean absolute peak errors. To assess the stub avoidance controller, we compared the prosthetic-side kinematics with and without extra flexion in terms of sagittal and frontal thigh angles, phase variables, and knee and ankle angles. Because vaulting (i.e., mid-stance plantarflexion of the intact-side ankle) is a common compensation to facilitate prosthesis ground clearance, we further quantified the frequency of vaulting using video recordings of every SA and LW trial.

To further assess stub avoidance during SA, we constructed two confusion matrices defined in Fig. S5. True positive (TP), false negative (FN), false positive (FP), and true negative

(TN) are marked on each confusion matrix. The accuracy of the simulated safe line was evaluated using data where the stub controller was disabled, and the effectiveness of the stub controller was evaluated using data where the subject stepped close to the next stairstep. For the safe line evaluation without the stub avoidance controller, stubs would ideally occur only when the participant steps close to the next stairstep. For the stub rate evaluation when stepping close to the stairs, stubs would ideally occur only when the stub avoidance controller is off. In addition, the controller evaluation matrix was used to calculate the stub rate (SR) with/without the stub avoidance controller (during risky steps) as follows:

$$\text{SR} = \begin{cases} \frac{\text{FP}}{\text{TP}+\text{FP}} & \text{if Stub Avoidance On,} \\ \frac{\text{TN}}{\text{TN}+\text{FN}} & \text{if Stub Avoidance Off} \end{cases} \quad (7)$$

We also evaluated the stub avoidance controller during obstacle crossing by calculating the stub rate by dividing the number of stub strides by the total number of obstacle crossing strides. To evaluate whether the proposed method can cross obstacles without delay due to the extra knee and ankle flexions, we compared the average stance and swing times between the obstacle crossing strides and normal walking strides, as recorded by the powered prosthetic leg.

To evaluate the FP rate of triggering extra flexion in the multi-activity simulation, we consider all the knee and ankle extra flexions that are greater than $3.56°$ and $2.33°$ (mean knee joint angle change that humans can perceive [51], [52]), respectively, as FPs. We then divided the number of FPs by the total number of strides to report the FP rate of triggering extra flexion during level/ramp walking. We also report the mean and standard deviation of FP extra flexions.

III. RESULTS

The following subsections summarize experimental results with two TF participants using a powered knee-ankle prosthesis with and without the stub avoidance controller during SA and LW. Summary statistics are presented for all participants, but for conciseness, the kinematics plots highlight a representative amputee participant, TF01. Refer to the Supplementary Materials for plots of TF02.

A. Baseline Kinematics

To assess biomimicry, we compare the baseline controller's kinematics (without extra joint flexion for stub avoidance) to the nominal AB data from an open-access dataset [44] for both SA and LW in Fig. 5 for TF01 and Fig. S2 for TF02. Fig. 5 also shows the participant's passive prosthesis data [53], [54]. The stair kinematics from the baseline controller follow the same pattern with similar magnitude as AB data, except for a phase shift due to the differences in thigh motion. In contrast, the passive leg data have a noticeable deviation from both nominal and powered prosthetic leg data. In the passive leg case, the thigh kinematics have a very large standard deviation before the mid-swing phase, and the ankle angle stays mostly constant indicating a lack of push-off assistance during SA. For LW, the mean kinematics from the baseline controller are mostly within one standard deviation of the AB
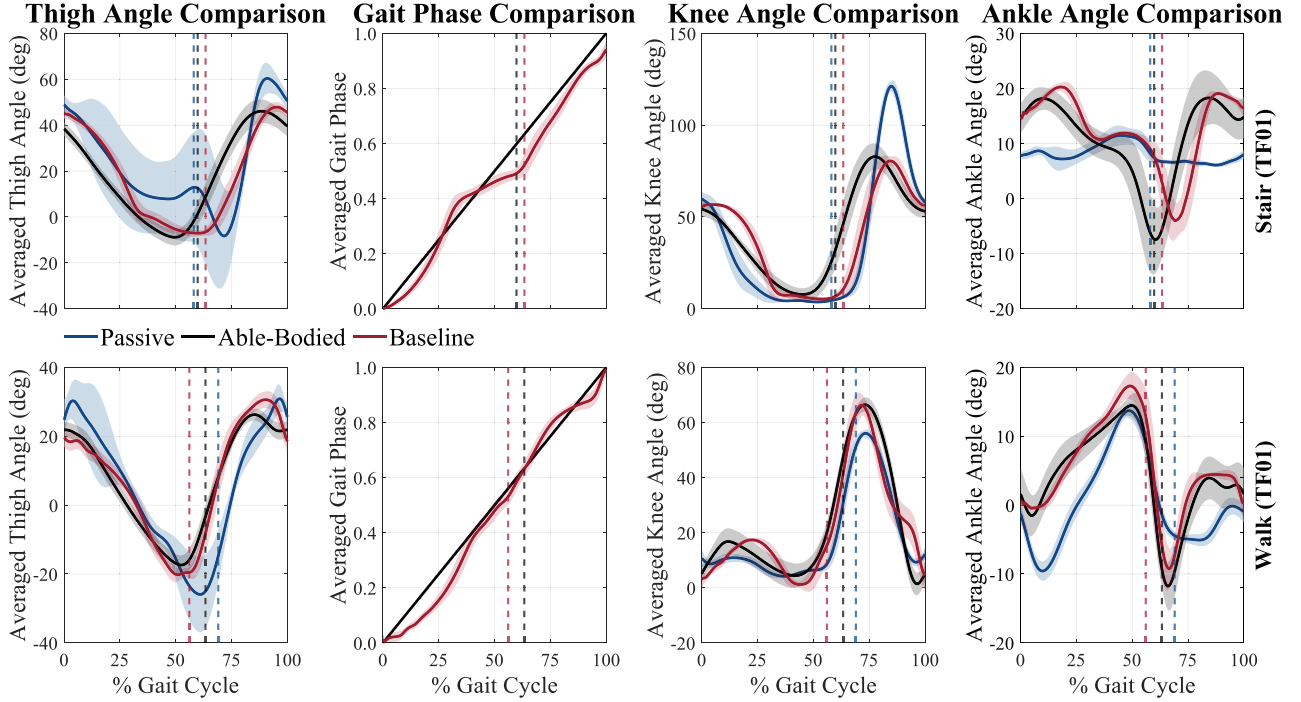
Fig. 5. Baseline controller kinematics comparison with able-bodied data for TF01. TF01's experimental results with the baseline controller compared with nominal able-bodied kinematics [44] for both stair ascending (first row) and level walking (second row). The solid black lines represent the ideal phase variable progression and the nominal kinematics, while the solid red lines show the results of the baseline controller. Kinematics using the participant's passive leg [53], [54] are plotted as blue solid lines. Shaded regions indicate ±1 standard deviation. The vertical lines demonstrate the average toe-off percentage gait cycle for the corresponding data. Positive kinematic values correspond to knee flexion or ankle dorsiflexion.

data for the knee and ankle joints, and the phase variable has a nearly linear trend with a slight lag during the early-mid stance phase. Although the thigh trajectory of passive leg walking has a similar shape to both AB and baseline, it demonstrates a higher thigh extension and later TO phase, indicating a shorter/faster swing phase than AB. Additionally, the passive ankle joint exhibits large plantarflexion (negative angle) during early stance and early swing when no angular displacement is expected.

Table S1 summarizes the mean and standard deviation of absolute kinematic errors at the maximum and minimum peak angles for the thigh, knee, and ankle of each participant to quantify the difference between the experimental and nominal data. For the powered prosthesis, the largest difference during SA ($3.92°$) and LW ($4.78°$) occurred at the knee and thigh joint, respectively, while the smallest difference during SA ($1.12°$) and LW ($0.82°$) both occurred at the ankle joint for both participants. The passive leg kinematics for TF01 exhibited a large difference from the nominal AB data during SA; the largest mean error ($39.45°$) occurred at the knee joint for the maximum peak. The passive leg caused higher peak error than the powered prosthetic leg over all joints for TF01 (more than 40 times higher at the knee joint).

B. Stub Avoidance Kinematics

The kinematics and phase variable for TF01 are compared between the baseline controller and the stub avoidance controller for both SA and LW in Fig. 6. Minimal hip com-

pensation can be observed in the average thigh trajectory during stub avoidance; this trajectory is largely within one standard deviation of the baseline controller, especially for SA. For SA stub avoidance, the thigh trajectory root-mean-square-error (RMSE) is $4.54 \pm 1.65°$ for TF01 and $3.69 \pm 1.62°$ for TF02. For obstacle crossing, because the kinematics are very similar across the two obstacle heights, they are pooled together for conciseness in the bottom row. The sagittal plane thigh trajectory shows a double peak near MHF that slightly overshoots the nominal peak thigh angle by $4.15°$ for TF01. The second row of Supplemental Fig. S3 shows a similar trend except the thigh angle difference near MHF is smaller ($3.03°$) for TF02. The thigh trajectory RMSE during LW obstacle avoidance is $5.34 \pm 1.64°$ for TF01 and $4.55 \pm 1.15°$ for TF02 when comparing LW without obstacle and stub avoidance with an obstacle. In addition, Fig. S4 highlights the minimal difference in the frontal-plane thigh trajectories (relating to hip abduction) between the baseline controller and stub avoidance controller.

The knee angle comparison in Fig. 6 shows the stub avoidance controller provided about $10°$ of extra flexion during SA and more than $40°$ of extra flexion to the baseline controller during LW obstacle crossing. A less noticeable change is added to the ankle during SA due to the large variation near the minimum peak, while approximately $10°$ of extra plantarflex-ion is observed during obstacle crossing. The joint angles of the baseline and stub avoidance controllers at HS match well for both cases. On average, TF01 and TF02 reach the
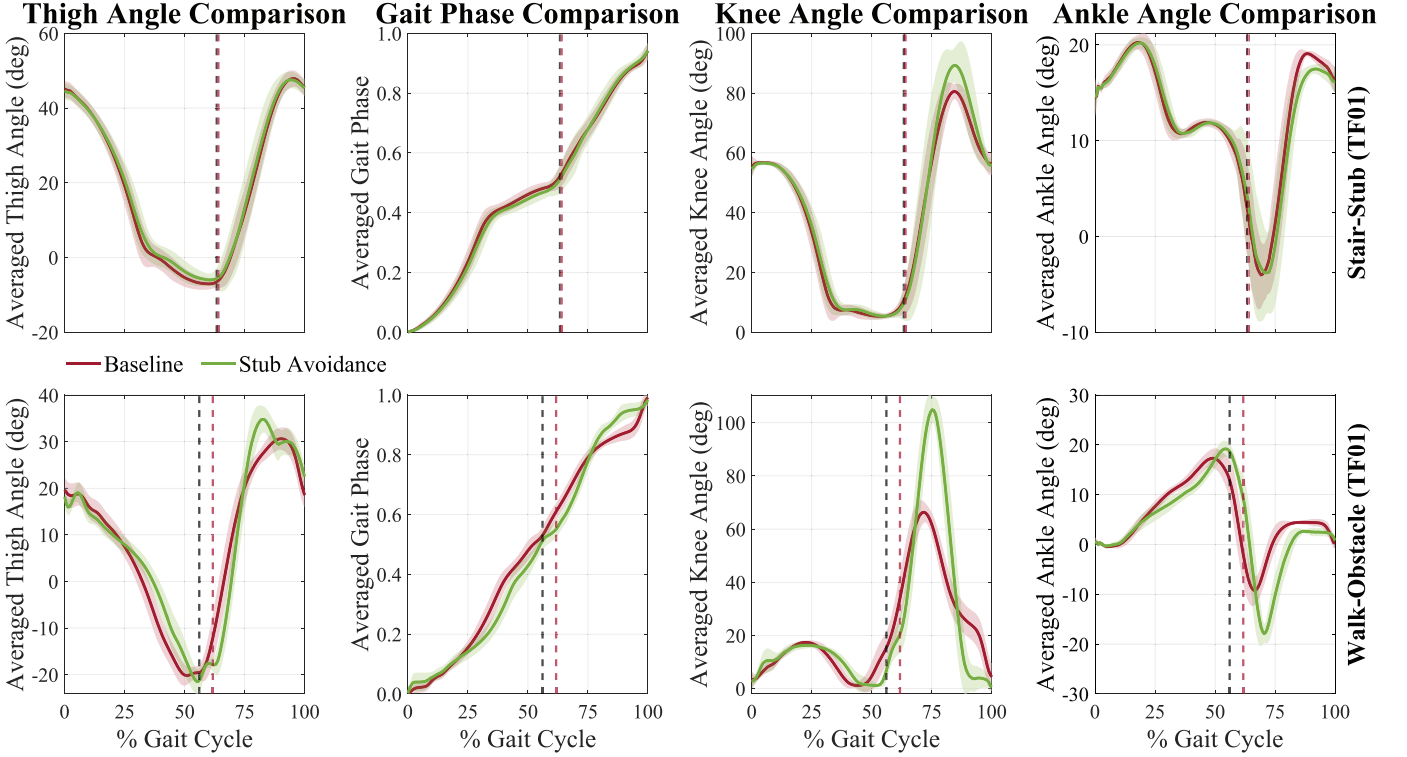
Fig. 6. Stub avoidance controller kinematics comparison with baseline controller for TF01. Comparison of TF01's kinematics and phase variable between baseline (red) and stub avoidance (green) controllers. The first row compares stair ascending with and without the stub avoidance controller (when no stub occurs), and the second row compares level walking with obstacle crossing on level ground. Shaded regions indicate ±1 standard deviation. Average toe-off percentage gait cycle are indicated as vertical lines in the figure. Positive kinematic values correspond to knee flexion or ankle dorsiflexion.

maximum knee flexion at $75.29 \pm 1.68\%$ and $73.96 \pm 0.96\%$ of the LW gait cycle, respectively, when the obstacle is present, compared to $71.69 \pm 2.13\%$ and $72.71 \pm 3.33\%$, respectively, when no obstacle is presented.

Fig. 7 shows a comparison of stance and swing time during LW with or without the presence of an obstacle. On average, the swing time was 24.9 ms longer with an obstacle for TF01. In contrast, TF02 had a negligible swing time difference less than 0.4 ms. Both participants exhibited longer stance time (TF01: +280.8 ms, TF02: +79.2 ms) with obstacles.

Finally, we observed a reduction in the frequency of intact-side vaulting during SA when the stub avoidance controller was on (54.8%) vs. off (65.9%) for TF02, who was the only participant to utilize this compensation during SA. We did not observe any such compensation during LW obstacle crossing with the stub avoidance controller.

C. Stub Avoidance Metrics

In the following subsections, we count any form of interaction between the prosthetic leg and stairs/obstacles during the swing phase as a stub, including kicking, scuffing, etc.

1) Stair Ascent: We first validate our experiment design (the ability to induce stair stubbing conditions) by evaluating the stub rate when stepping in front of vs. behind the safe line (close vs. far from the next stairstep) with the baseline controller. The results are given in the confusion matrices of Fig. 8(A). As expected, we see a reasonably high rate of TP, meaning a stub occurred because the participant stepped in
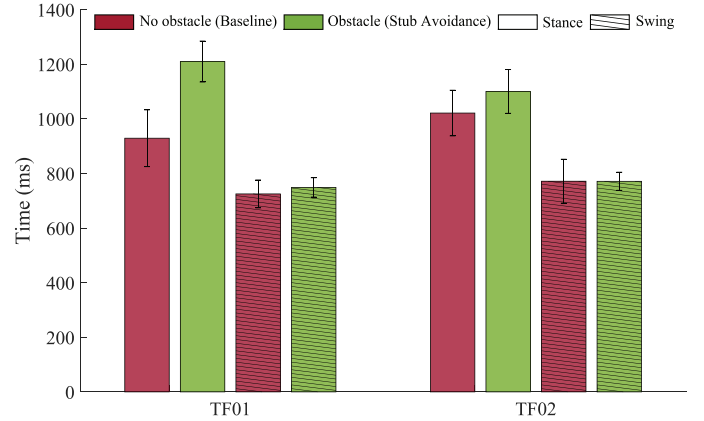

Fig. 7. Stance and swing time comparison. Stance and swing time for level walking with and without obstacles for each participant. The error bar represents ± 1 standard deviation.

front of the safe line (49.09% on average), with a similar rate of FP, meaning no stub occurred despite stepping in front of the safe line (50.91% on average). We also see a high rate of TN, meaning no stub occurred when stepping safely behind the safe line (93.55% on average), and a low rate of FN, meaning a stub occurred despite stepping far from the next stairstep (6.45% on average). These results indicate that, by instructing participants to step in front of the safe line during SA, our experimental protocol can induce a high risk of stubbing for the purpose of evaluating the stub avoidance controller.
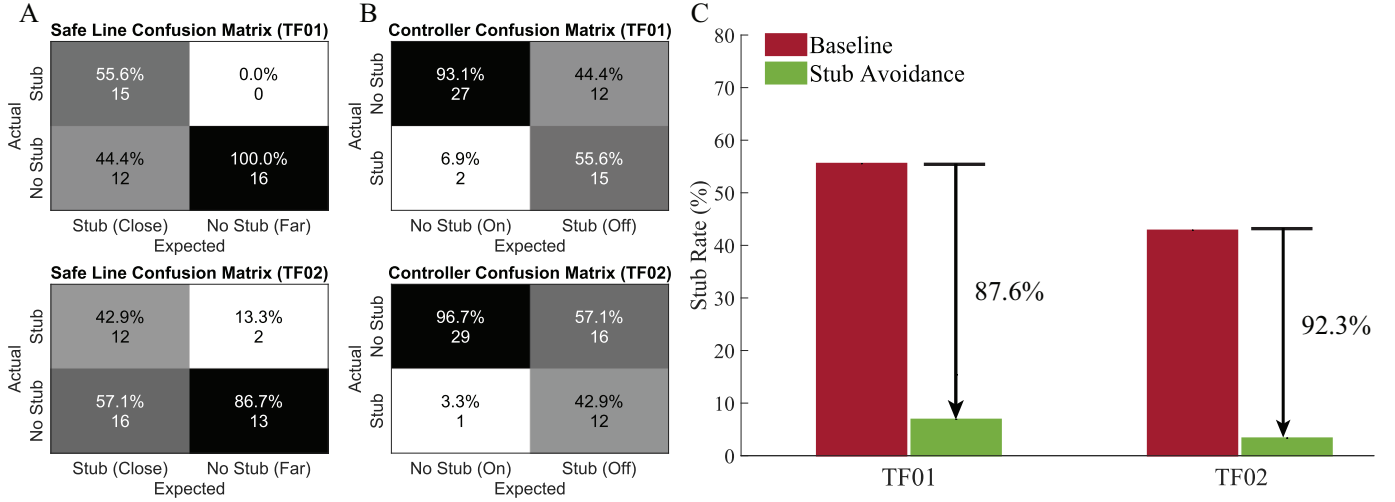
Fig. 8. Confusion matrices and bar chart for stub rates during stair ascending. (A) quantifies the experimental accuracy of the simulated safe line when the stub controller was disabled, highlighting the high stub rate (TF01: 55.60%, TF02: 42.90%) when placing the prosthetic foot close to the next stairstep. (B) quantifies the stub rates with and without the stub avoidance controller (On vs. Off) when the subject intentionally steps close to the next stairstep, highlighting the low stub rate (TF01: 6.90%, TF02: 3.30%) with the stub avoidance controller. (C) Stub rate comparison between baseline (red) and stub avoidance (green) controllers when the prosthetic foot is close to the next stairstep, i.e., in front of the safe line.

The effectiveness of the stub avoidance controller is evaluated by the stub rate when stepping in front of the safe line with or without the stub avoidance controller. This protocol restricts our analysis to high risk conditions where the stub avoidance controller is most necessary, but does not allow analysis of undesirable "false" activations of the stub avoidance controller (which will be considered later). The confusion matrices of Fig. 8(B) show a very high TP rate (94.92% on average), meaning the stub avoidance controller successfully avoided a stub, with a very low FP rate (5.08% on average), where the stub avoidance controller failed to prevent a stub. The rate of TN, meaning a stub occurred as expected because the stub avoidance controller was off, matches the TP rate (49.09% on average) for the safe line evaluation in Fig. 8(A), which indeed correspond to the same experimental condition. Similarly, the rate of FN, meaning no stub occurred despite the stub controller being off, matches the FP rate (50.91% on average) for the safe line evaluation in Fig. 8(A).

Finally, Fig. 8(C) shows the stub avoidance controller reduced the stub rate by 87.6% for TF01 and 92.3% for TF02.

2) Obstacle Crossing: For the obstacle crossing experiment, each participant performed 16 trials of successful obstacle crossings, despite a toe stub rate of 0% for TF01 and 25% for TF02. TF02 scuffed twice on each of the 4.75-inch and 6.75-inch obstacles but was still able to cross the obstacles in all cases.

3) Robustness in a Multi-Activity Circuit: We further evaluated the robustness of the stub avoidance controller in an offline simulation with pre-recorded ultrasonic data from a multi-activity circuit including sitting, standing, level and ramp walking, turning, stair ascending/descending, and transitions between them in a relatively narrow lab environment, all *without obstacles*. In our prior work [50], TF01 was instructed to perform as many continuous laps of these activities as possible, providing 660 strides for our analysis. We simulated

the stub avoidance controller's output to check whether extra flexion would be falsely triggered during these activities. Because the stub avoidance controller can produce a continuous range of extra flexion depending on the distance measurement (including very small values), we classified false events by extra flexion greater than $3.56°$ for the knee and $2.33°$ for the ankle, which correspond to the minimal perceptible changes in those joint angles by AB [51], [52]. The overall FP rate was 1.23%, where those false events produced on average $10.22 \pm 5.20°$ of extra flexion for the knee (extra ankle flexion is proportional to the knee by scaling factor -0.25). All occurrences of extra flexion, including false events, returned the knee trajectory back to nominal value by HS.

IV. Discussion

A. Biomimicry of Baseline Controller

The similarity between the experimental kinematics and nominal AB kinematics (Figs. 5-6, Figs. S2-S4) indicates that the baseline controller of the powered prosthetic leg restored a reasonably normative gait for the amputee users. For SA, the higher peak flexion and large standard deviation in residual thigh motion when TF01 used the passive prosthesis to climb stairs indicate they compensated with their hip to clear the step due to the non-biomimetic knee and ankle kinematics. In particular, the user extended the thigh backward after TO causing the large second minimum in Fig. 5 and then rapidly flexed the thigh to trigger prosthetic knee flexion during the early swing phase, which is reported as an effective compensatory strategy to avoid tripping during SA [55]. This behavior was not necessary with the powered prosthetic leg, but this came with a risk of stubbing when stepping close to a stairstep without active stub avoidance (Fig. 8). The difference is even more significant for TF02, who was unable to perform step-over-step SA with their passive prosthesis,

instead adopting a step-to-step gait (not shown because we excluded this style of SA gait from the protocol).

The phase variable of the baseline controller in Fig. 5 shows a flat region corresponding to slower thigh movement during the late stance of SA, which reflects the user's thigh motion pausing at this point of the gait cycle. This could be the result of participants visually inspecting their foot placement to achieve the instructed position and/or a compensation strategy from the habitual use of their passive device to swing the prosthetic leg backward after TO. This pause in the phase variable, which caused a corresponding pause in the prosthetic joint patterns, explains the phase shift seen with respect to AB joint kinematics over normalized time (% gait cycle).

For LW, the baseline controller kinematics closely resemble the nominal AB kinematics while the passive kinematics do not. The passive knee kinematics do not reach the desired maximum flexion, which is critical to generate enough foot clearance. Therefore, more compensation is expected if the participant wants to step over obstacles with the passive leg.

In most cases, the mean absolute errors of the minimum peaks between the prosthetic and AB joint kinematics (Table S1) are smaller than the variation in joint angles that AB individuals can perceive (knee $\approx 3.56°$ [51], ankle $\approx 2.33°$ [52]) for both SA and LW. While the knee joint shows the same trend for the maximum peak, the ankle joint shows higher mean peak errors for both participants. This can be explained by the higher tracking error in the ankle joint during the stance phase in Supplemental Fig. S1. In addition, the kinematics models [23] that were used to compute the desired joint angles of the baseline controller have a maximum mean fitting RMSE of 2.21° and 0.94° for the knee and ankle joints, respectively, which could also contribute to the peak error in Table S1.

B. Stub Avoidance Controller Performance

1) Kinematics: For both participants, the thigh motions during SA (Fig. 6, Fig. S3) were almost equivalent with and without the stub avoidance controller, indicating the participants required no compensations to utilize the extra joint flexion. Therefore, the phase variable, knee, and ankle kinematics are very similar except for the extra flexion added to the knee and ankle joints. The extra flexion stopped at about 85% of the gait cycle to allow normal foot placement on the next stairstep. Moreover, the observed reduction in the frequency of intact-side vaulting with the stub avoidance controller for TF02 suggests that the proposed method may help reduce intact-side compensations commonly used to facilitate ground clearance.

Obstacle crossing exhibited thigh motion that was comparable to normal LW except for an earlier, larger peak at MHF before returning to the normative peak (Fig. 6). The mean discrepancy of 3.59° could be the result of the participant's intention to raise the thigh and step over the obstacle, or the knee torque required to achieve 40° of extra flexion may have caused a reaction torque at the hip. This double peak caused a slightly faster progression of phase near MHF. Near MHE, we observed a smaller double peak in the thigh angle and a delay of the average TO phase, which could be due to a

distinct obstacle-crossing motion of the intact leg. Following obstacle crossing, the joint angles at HS matched normal walking, allowing the next step to continue as usual. With minimal thigh angle differences in both the sagittal (Fig. 6 and Fig. S3) and frontal planes (Fig. S4), participants were able to cross obstacles and stairs without substantial thigh kinematic compensations. Moreover, we did not observe vaulting during LW obstacle crossing, whereas Mendez et al. demonstrated that exaggerated vaulting motions are commonly used by passive prosthesis users to clear obstacles [17].

According to Fig. 7, our controller allowed the TF participants to cross obstacles without extra swing time. Because the stub avoidance controller anticipated the amount of extra swing flexion based on ultrasonic readings during the preceding stance phase, the knee could start flexing as soon as TO with increasing angular velocity to reach the maximum flexion. This demonstrated a more natural and expedient way to cross obstacles compared to the method proposed in [17], where longer swing times were required for the thigh angle integral to generate enough knee flexion.

2) Avoidance Rate: Overall, the safe line evaluation with the baseline controller in Fig. 8(A) shows a 12.1% probability of stubbing during SA when the foot was placed behind the line, whereas the risk was more than 4 times higher (49.09%) when stepping in front of the line. This baseline stub rate was lower for TF02 (42.90%) than TF01 (55.60%) mainly because of the former's vaulting motion from the intact leg to generate more ground clearance. Other compensations, such as hip circumduction, could also contribute to the stub rates of TF participants. The high stub rates demonstrate the importance of the stub avoidance controller, which reduced the overall stub rate from 49.09% to 5.08% (Fig. 8(B) and Fig. 8(C)) during risky stepping conditions. Although TF01 was able to achieve a similar stub rate during passive leg trials with *normal* stepping conditions, it required significant hip compensations shown in Fig. 5 (blue lines) to avoid stair stubbing. With our stub avoidance controller, the participant achieved a comparable avoidance rate during *risky* stepping conditions without any extra thigh motion (Fig. 6).

Although the stub avoidance controller generated enough clearance to cross the obstacle without kicking it in all trials, a few scuffs were observed with TF02 and counted as stubs. After completing the first participant (TF02), we realized the knee velocity's rate limit of $350°\,s^{-1}$ was too conservative when walking at a fast speed. Hence, the extra knee flexion was too slow in some of TF02's trials. After we increased the rate limit to $500°\,s^{-1}$ for TF01, we successfully achieved a 0% stub rate for both obstacle heights.

The offline simulation results in Section III-C3 demonstrate the robustness of the stub avoidance controller in daily locomotion with a low FP rate (1.23%) for triggering extra flexion when no obstacle is presented in multiple activities. For those FP strides, the extra flexions gradually returned back to 0 around 80% of the gait cycle, ensuring the prosthetic foot is in a good position at HS. In addition, previous studies have shown negligible effects of kinematic differences in early to mid-swing on gait stability during level and ramp walking [56], [57], which further reduces the risk of FP stub avoidance

flexion.

C. Limitations and Future Work

This study has several limitations. First, this proof-of-concept case study only included two participants, which is insufficient to perform statistical analysis and confirm the generalizability of the proposed method to the broader population. Second, our stub avoidance controller assumed the highest step/obstacle height because the current sensor configuration cannot measure stair/obstacle height, resulting in excess flexion for the lower obstacle height. Possible solutions include 1) estimating obstacle height using its correlation with the thigh angle at MHF, or 2) using a closed-loop distance feedback controller during swing. Third, the stub avoidance controller is open-loop due to the low sampling frequency of the ultrasonic sensors (40 Hz) and the measurement noise when pointing towards uneven surfaces. Although the distance measurement was filtered to reduce noise, jumps in the ultrasonic signal were still observed for a few strides of data, especially during SA. Therefore, we used a conservative safe distance to calculate extra flexion on stairs, which resulted in possibly unnecessary flexion when stepping far enough from the stairstep. Using a more reliable ultrasonic sensor with a higher sampling frequency may resolve these issues. Fourth, the proposed sensor setup (6.35 cm above the ankle) would require the user to roll up long pants to prevent blocking the ultrasonic sensor. Alternatively, the small ultrasonic sensor could be relocated to the shoe. Finally, the study did not address stubs during stair descent, which would require fast and accurate measurements of distance from the stair riser behind the prosthetic foot during swing phase.

Future work includes validating the controller on more amputee participants to determine clinical outcomes, analyzing the intact-side kinematics, extracting stair/obstacle height as an additional input to the stub avoidance controller, and performing closed-loop distance tracking. In addition, we could consider replacing the ultrasonic sensor as LiDAR sensors become smaller, cheaper, and more efficient for mobile applications, which could provide more environmental features (like step/obstacle height, depth, etc.). Finally, distance sensing also provides a good measurement range and could provide useful time-series data for detecting changes in the approaching terrain, motivating future work in activity classification including early detection of activity transition strides.

V. CONCLUSIONS

This paper presented an ultrasonic distance-based kinematics modification method for automatic stub avoidance on top of a baseline controller that restores nominal able-bodied kinematics for amputee users. The stub avoidance controller reduced the stub rate by about 90% during risky stair stepping conditions (associated with approximately 50% chance of stubbing without active avoidance). The stub avoidance controller also enabled obstacle crossing through sufficient extra knee flexion, with only minor scuffs contributing to the 12.5% stub rate. The stub avoidance controller had a negligible effect on the motion of the residual hip and in fact reduced

ankle vaulting on the sound side, demonstrating that kinematic compensations were not required to clear steps and obstacles.

REFERENCES

[1] A. Vrieling, H. van Keeken, T. Schoppen, E. Otten, J. Halbertsma, A. Hof, and K. Postema, "Obstacle crossing in lower limb amputees," *Gait Posture*, vol. 26, pp. 587–594, 11 2007.

[2] B. J. Hafner, L. L. Willingham, N. C. Buell, K. J. Allyn, and D. G. Smith, "Evaluation of function, performance, and preference as transfemoral amputees transition from mechanical to microprocessor control of the prosthetic knee," *Arch. Phys. Med. Rehabil.*, vol. 88, no. 2, pp. 207–217, 2007.

[3] J. T. Kahle, M. J. Highsmith, S. L. Hubbard *et al.*, "Comparison of nonmicroprocessor knee mechanism versus c-leg on prosthesis evaluation questionnaire, stumbles, falls, walking tests, stair descent, and knee preference," *J. Rehabil. Res. Dev.*, vol. 45, no. 1, p. 1, 2008.

[4] M. Eveld, S. King, K. Zelik, and M. Goldfarb, "Factors leading to falls in transfemoral prosthesis users: a case series of sound-side stumble recovery responses," *J. NeuroEng. Rehabil.*, vol. 19, pp. 1–24, 09 2022.

[5] H. Hobara, Y. Kobayashi, T. Nakamura, N. Yamasaki, K. Nakazawa, M. Akai, and T. Ogata, "Lower extremity joint kinematics of stair ascent in transfemoral amputees," *Prosthet. Orthot. Int.*, vol. 35, pp. 467–472, 12 2011.

[6] J. Lee and M. Goldfarb, "Effect of a swing-assist knee prosthesis on stair ambulation," *IEEE Trans. Neural Syst. Rehabil. Eng.*, vol. 29, pp. 2046–2054, 09 2021.

[7] D. Ehde, D. Smith, J. Czerniecki, K. Campbell, D. Malchow, and L. Robinson, "Back pain as a secondary disability in persons with lower limb amputations," *Arch. Phys. Med. Rehabil.*, vol. 82, pp. 731–734, 06 2001.

[8] F. Sup, H. A. Varol, and M. Goldfarb, "Upslope walking with a powered knee and ankle prosthesis: Initial results with an amputee subject," *IEEE Trans. Neural Syst. Rehabil. Eng.*, vol. 19, no. 1, pp. 71–78, 2011.

[9] B. E. Lawson, H. A. Varol, A. Huff, E. Erdemir, and M. Goldfarb, "Control of stair ascent and descent with a powered transfemoral prosthesis," *IEEE Trans. Neural Syst. Rehabil. Eng.*, vol. 21, no. 3, pp. 466–473, 2013.

[10] C. Jayaraman, S. Hoppe-Ludwig, S. Deems-Dluhy, M. McGuire, C. Mummidisetty, R. Siegal, A. Naef, B. E. Lawson, M. Goldfarb, K. E. Gordon *et al.*, "Impact of powered knee-ankle prosthesis on low back muscle mechanics in transfemoral amputees: A case series," *Frontiers Neuroscience*, vol. 12, pp. 1–13, 2018.

[11] T. Elery, S. Rezazadeh, C. Nesler, and R. D. Gregg, "Design and validation of a powered knee–ankle prosthesis with high-torque, low-impedance actuators," *IEEE Trans. Robot.*, vol. 36, no. 6, pp. 1649–1668, 2020.

[12] E. Lathouwers, M. Díaz, A. Maricot, B. Tassignon, C. Cherelle, P. Cherelle, R. Meeusen, and K. De Pauw, "Therapeutic benefits of lower limb prostheses: a systematic review," *J. NeuroEng. Rehabil.*, vol. 20, pp. 1–27, 01 2023.

[13] R. Gehlhar, M. Tucker, A. J. Young, and A. D. Ames, "A review of current state-of-the-art control methods for lower-limb powered prostheses," *Annual Reviews in Control*, 2023.

[14] S. Rezazadeh, D. Quintero, N. Divekar, E. Reznick, L. Gray, and R. D. Gregg, "A phase variable approach for improved rhythmic and non-rhythmic control of a powered knee-ankle prosthesis," *IEEE Access*, vol. 7, pp. 109 840–109 855, 2019.

[15] M. Li, W. Liu, J. Si, J. Stallrich, and H. Huang, "Hierarchical optimization for control of robotic knee prostheses toward improved symmetry of propulsive impulse," *IEEE Trans. Biomed. Eng.*, pp. 1–9, 2022.

[16] T. K. Best, C. G. Welker, E. J. Rouse, and R. D. Gregg, "Data-driven variable impedance control of a powered knee–ankle prosthesis for adaptive speed and incline walking," *IEEE Trans. Robot.*, pp. 1–19, 2023.

[17] J. Mendez, S. Hood, A. Gunnel, and T. Lenzi, "Powered knee and ankle prosthesis with indirect volitional swing control enables level-ground walking and crossing over obstacles," *Sci. Robot.*, vol. 5, p. eaba6635, 07 2020.

[18] B. J. Hafner and R. L. Askew, "Physical performance and self-report outcomes associated with use of passive, adaptive, and active prosthetic knees in persons with unilateral, transfemoral amputation: Randomized crossover trial." *J. Rehabil. Res. Dev.*, vol. 52, no. 6, 2015.

[19] T. Killeen, C. S. Easthope, L. Demkó, L. Filli, L. Lőrincz, M. Linnebank, A. Curt, B. Zörner, and M. Bolliger, "Minimum toe clearance: probing the neural control of locomotion," *Scientific reports*, vol. 7, no. 1, p. 1922, 2017.

[20] S. Beausoleil, L. Miramand, and K. Turcot, "Evolution of gait parameters in individuals with a lower-limb amputation during a six-minute walk test," *Gait Posture*, vol. 72, pp. 40–45, 2019.

[21] N. Lythgo, R. Begg, and R. Best, "Stepping responses made by elderly and young female adults to approach and accommodate known surface height changes," *Gait Posture*, vol. 26, pp. 82–89, 06 2007.

[22] N. Rokhmanova and E. Rombokas, "Vibrotactile feedback improves foot placement perception on stairs for lower-limb prosthesis users," in *IEEE 16th Int. Conf. Rehabil. Robot. (ICORR)*, 2019, pp. 1215–1220.

[23] S. Cheng, E. Bolívar-Nieto, C. G. Welker, and R. D. Gregg, "Modeling the transitional kinematics between variable-incline walking and stair climbing," *IEEE Trans. Med. Robot. Bionics*, vol. 4, no. 3, pp. 840–851, 2022.

[24] B. Lawson, A. Varol, F. Sup IV, and M. Goldfarb, "Stumble detection and classification for an intelligent transfemoral prosthesis," *Proc. IEEE Annu. Int. Conf. Eng. Med. Biol. Soc.*, vol. 2010, pp. 511–514, 08 2010.

[25] F. Zhang, S. D'Andrea, M. Nunnery, S. Kay, and H. Huang, "Towards design of a stumble detection system for artificial legs," *IEEE Trans. Neural Syst. Rehabil. Eng.*, vol. 19, pp. 567–577, 08 2011.

[26] N. Thatte and H. Geyer, "Toward balance recovery with leg prostheses using neuromuscular model control," *IEEE Trans. Biomed. Eng.*, vol. 63, no. 5, pp. 904–913, 2016.

[27] M. Gordon, N. Thatte, and H. Geyer, "Online learning for proactive obstacle avoidance with powered transfemoral prostheses," in *Int. Conf. Robot. Autom. (ICRA)*, 2019, pp. 7920–7925.

[28] S. Hood, L. Gabert, and T. Lenzi, "Powered knee and ankle prosthesis with adaptive control enables climbing stairs with different stair heights, cadences, and gait patterns," *IEEE Trans. Robot.*, vol. 38, no. 3, pp. 1430–1441, 2022.

[29] M. Liu, D. Wang, and H. Huang, "Development of an environment-aware locomotion mode recognition system for powered lower limb prostheses," *IEEE Trans. Neural Syst. Rehabil. Eng.*, vol. 24, no. 4, pp. 434–443, 2016.

[30] B. Laschowski, W. McNally, A. Wong, and J. McPhee, "Preliminary design of an environment recognition system for controlling robotic lower-limb prostheses and exoskeletons," in *IEEE 16th Int. Conf. Rehabil. Robot. (ICORR)*, 2019, pp. 868–873.

[31] J. P. Diaz, R. L. da Silva, B. Zhong, H. H. Huang, and E. Lobaton, "Visual terrain identification and surface inclination estimation for improving human locomotion with a lower-limb prosthetic," in *2018 40th Annual International Conference of the IEEE Engineering in Medicine and Biology Society (EMBC)*, 2018, pp. 1817–1820.

[32] B. Zhong, R. L. d. Silva, M. Tran, H. Huang, and E. Lobaton, "Efficient environmental context prediction for lower limb prostheses," *IEEE Trans. Systems, Man, and Cybernetics: Systems*, vol. 52, no. 6, pp. 3980–3994, 2022.

[33] M. Tschiedel, M. F. Russold, E. Kaniusas, and M. Vincze, "Real-time limb tracking in single depth images based on circle matching and line fitting," *The Visual Computer*, vol. 38, no. 8, pp. 2635–2645, 2022.

[34] K. Zhang, J. Luo, C. Fu, W. Xiao, W. Zhang, H. Liu, J. Zhu, Z. Lu, Y. Rong, and C. Silva, "A subvision system for enhancing the environmental adaptability of the powered transfemoral prosthesis," *IEEE Trans. Cybern.*, vol. 51, no. 6, pp. 3285–3297, 03 2020.

[35] M. A. Contreras-Cruz, L. Novo-Torres, D. J. Villarreal, and J.-P. Ramirez-Paredes, "Convolutional neural network and sensor fusion for obstacle classification in the context of powered prosthetic leg applications," *Comput. Elect. Eng.*, vol. 108, p. 108656, 2023.

[36] N. Thatte, N. Srinivasan, and H. Geyer, "Real-time reactive trip avoidance for powered transfemoral prostheses." in *Robotics: Science and Systems*, 2019.

[37] B. Laschowski, W. McNally, A. Wong, and J. McPhee, "Environment classification for robotic leg prostheses and exoskeletons using deep convolutional neural networks," *Frontiers in Neurorobotics*, vol. 15, p. 730965, 2022.

[38] J. Zaczek-Peplinska and M. Kowalska, "Evaluation of the lidar in the apple iphone 13 pro for use in inventory works," Department of Engineering Geodesy and Control Surveying Systems, Tech. Rep., 2022.

[39] C. Linnhoff, K. Hofrichter, L. Elster, P. Rosenberger, and H. Winner, "Measuring the influence of environmental conditions on automotive lidar sensors," *Sensors*, vol. 22, no. 14, p. 5266, 2022.

[40] J. Jiang, G. Cao, J. Deng, T.-T. Do, and S. Luo, "Robotic perception of transparent objects: A review," *arXiv preprint arXiv:2304.00157*, 2023.

[41] V. Zhmud, N. Kondratiev, K. Kuznetsov, V. Trubin, and L. Dimitrov, "Application of ultrasonic sensor for measuring distances in robotics," *J. Physics: Conf. Series*, vol. 1015, pp. 1–9, 05 2018.

[42] A. Carullo and M. Parvis, "An ultrasonic sensor for distance measurement in automotive applications," *IEEE Sensors J.*, vol. 1, pp. 143 – 147, 09 2001.

[43] A. Ruíz-Serrano, M. C. Reyes-Fernández, R. Posada-Gómez, A. Martínez-Sibaja, and A. A. Aguilar-Lasserre, "Obstacle avoidance embedded system for a smart wheelchair with a multimodal navigation interface," in *Int. Conf. Elect. Eng. Comput. Sci. Autom. Control*, 2014.

[44] E. Reznick, K. Embry, R. Neuman, E. Bolívar-Nieto, N. Fey, and R. Gregg, "Lower-limb kinematics and kinetics during continuously varying human locomotion," *Sci. Data*, vol. 8, pp. 1–12, 10 2021.

[45] R. J. Cortino, E. Bolívar-Nieto, T. K. Best, and R. D. Gregg, "Stair ascent phase-variable control of a powered knee-ankle prosthesis," in *IEEE Int. Conf. Robot. Autom.*, 2022, pp. 5673–5678.

[46] D. Quintero, D. Villarreal, D. Lambert, S. Kapp, and R. Gregg, "Continuous-phase control of a powered knee-ankle prosthesis: Amputee experiments across speeds and inclines," *IEEE Trans. Robot.*, vol. 34, no. 3, pp. 686–701, 2018.

[47] D. J. Villarreal, H. A. Poonawala, and R. D. Gregg, "A robust parameterization of human gait patterns across phase-shifting perturbations," *IEEE Trans. Neural Syst. Rehabil. Eng.*, vol. 25, no. 3, pp. 265–278, 2017.

[48] W. Hong, N. A. Kumar, and P. Hur, "A phase-shifting based human gait phase estimation for powered transfemoral prostheses," *IEEE Robot. Autom. Lett.*, vol. 6, no. 3, pp. 5113–5120, 2021.

[49] S. Cheng, E. Bolívar-Nieto, and R. D. Gregg, "Real-time activity recognition with instantaneous characteristic features of thigh kinematics," *IEEE Trans. Neural Syst. Rehabil. Eng.*, vol. 29, pp. 1827–1837, 2021.

[50] T. K. Best, C. A. Laubscher, R. J. Cortino, S. Cheng, and R. D. Gregg, "Improving Amputee Endurance over Activities of Daily Living with a Robotic Knee-Ankle Prosthesis: A Case Study," *IEEE Int. Conf. Intelli. Robot. Sys.*, 2023.

[51] D. Barrett, A. Cobb, and G. Bentley, "Joint proprioception in normal osteoarthritic and replaced knees," *J. Bone Joint Surg. Brit.*, vol. 73, pp. 53–56, 02 1991.

[52] N. Deshpande, D. M. Connelly, E. G. Culham, and P. A. Costigan, "Reliability and validity of ankle proprioceptive measures," *Arch. Phys. Med. Rehabil.*, vol. 84, pp. 883–889, 6 2003.

[53] R. J. Cortino, T. K. Best, and R. D. Gregg, "Data-Driven Phase-Based Control of a Powered Knee-Ankle Prosthesis for Variable-Incline Stair Ascent and Descent," *IEEE Trans. Medical Robotics and Bionics*, 2023.

[54] C. Welker, T. K. Best, and R. Gregg, "Improving Sit/Stand Loading Symmetry and Timing Through Unified Variable Impedance Control of a Powered Knee-Ankle Prosthesis," *IEEE Trans. Neural Syst. Rehabil. Eng.*, 2023.

[55] H. Hobara, Y. Kobayashi, T. Nakamura, N. Yamasaki, and T. Ogata, "Foot clearance strategy for step-over-step stair climbing in transfemoral amputees," *Prosthet. Orthot. Int.*, vol. 38, pp. 332–335, 08 2013.

[56] F. Zhang, M. Liu, and H. Huang, "Effects of locomotion mode recognition errors on volitional control of powered above-knee prostheses," *IEEE Trans. Neural Syst. Rehabil. Eng.*, vol. 23, no. 1, pp. 64–72, 2014.

[57] ——, "Investigation of timing to switch control mode in powered knee prostheses during task transitions," *PloS one*, vol. 10, p. e0133965, 2015.